ARTICLE NO. 80-4073

A 80-055

Hypersonic Viscous Shock-Layer Flows Including Leeside Separation

20005
20017
20019

P. R. Gogineni* and Clark H. Lewis†
Virginia Polytechnic Institute and State University, Blacksburg, Va.
and
Bohdan Denysyk‡
EG&G, Dahlgren, Va.

The three-dimensional, laminar, viscous hypersonic flowfield over blunted cones at large angles of attack, including crossflow separation, has been solved using both viscous shock-layer and parabolized Navier-Stokes equations. A computer code has been developed using this technique, and calculations were made for two test cases, which typically encompass laminar re-entry flow conditions. Case 1 considered low Mach number (10) and high Reynolds number (2×10^6/ft) at moderate angle of attack (10 deg). Case 2 considered high Mach number (25) and low Reynolds number (7256/ft) at large angle of attack (35 deg). The results have been compared with a complete parabolized Navier-Stokes solution, and for case 1, the aerodynamic coefficients have been compared with available experimental data. The comparisons indicate good agreement for wall pressure, both longitudinal and crossflow skin-friction coefficients and aerodynamic coefficients. A fast implicit iterative technique known as the Pseudo Elimination Method has been used to solve the parabolized Navier-Stokes equations, and the computing time has been reduced by 35%. The computing times required indicate that the present code obtains complete flowfield solutions in the shortest possible time, thus making it an ideal tool for design analysis of lifting re-entry vehicles.

Nomenclature

C_a = axial force coefficient
C_{f_s} = streamwise skin-friction coefficient
C_{f_ϕ} = crossflow skin-friction coefficient
C_m = pitching moment coefficient
C_n = normal force coefficient
C_p = pressure coefficient
c_p = specific heat at constant pressure, $ft^2/s^2 - °R$
h = static enthalpy $= h^*/U_\infty^2$
K = number of grid points in the normal direction
k = counter in the normal direction
L = number of grid points in the ϕ direction
l = counter in the ϕ direction
M = Mach number
n_{sh} = shock-layer thickness in n direction
p = pressure $= p^*/\rho_\infty U_\infty^2$
Re = Reynolds number $= \rho_\infty U_\infty R_n^*/\mu_\infty$
R_n^* = nose radius, ft
s,n,ϕ = surface-oriented normal coordinate system, s and n nondimensionalized by nose radius R_n^*
T = temperature $= T^*/T_{ref}^*$
T_{ref}^* = reference temperature $= U_\infty^2/c_p^*$
U_∞ = freestream velocity, ft/s
u,v,w = velocity components $= u^*/U_\infty$, v^*/U_∞, w^*/U_∞
x,r,ϕ = cylindrical coordinate system
x,y,z = Cartesian coordinate system
α = angle of attack, deg
β = shock-layer thickness in parabolized Navier-Stokes solution
γ = ratio of specific heats
ϵ = Reynolds number parameter $= (\mu_{ref}^*/\rho_\infty U_\infty R_n^*)^{1/2}$
μ = viscosity $= \mu^*/\mu_{ref}^*$
$\xi1,\xi2,\xi3$ = body-normal coordinate system
ρ = density $= \rho^*/\rho_\infty$

Subscripts

∞ = dimensional freestream conditions
sh = conditions behind the bow shock

Superscript

$(\,)^*$ = dimensional quantity

Received June 25, 1979; revision received Dec. 10, 1979.

Index categories: Viscous Nonboundary-Layer Flows; Computational Methods; Supersonic and Hypersonic Flow.

*Research Fellow, Aerospace and Ocean Engineering Dept; currently at Lockheed Missile and Space Co., Sunnyvale, Calif. Member AIAA.

†Professor, Aerospace and Ocean Engineering Dept. Associate Fellow AIAA.

‡Head, Technical Assessment and Analysis Dept. Member AIAA.

Introduction

CONTINUED interest in the design of lifting re-entry vehicles motivates the efforts to develop a computer code to solve the complex three-dimensional viscous hypersonic flowfield in reasonable computing times, such that it could be used as a tool in design analysis. Re-entry vehicles encounter a wide range of flow conditions at high angles of attack, and the resulting complex flowfield is sketched in Fig. 1. The flowfield is bounded by the body as the inner boundary and the bow shock as the outer boundary. The crossflow separates on the leeward side, and viscous effects are predominant over the entire flowfield. The analytical treatment of this complex flowfield requires the solution of full Navier-Stokes equations which are elliptic in all three space dimensions, making their numerical solution difficult and requiring large amounts of storage and computer time even on today's computers. The classical approach divided the flowfield into two regions; namely, the inviscid outer flow and the viscous boundary-layer flow, assuming that the viscous effects were limited to the boundary layer. The treatment of outer boundary conditions for the boundary-layer flow was difficult, but has been approximated by using inviscid-viscous iterative-type

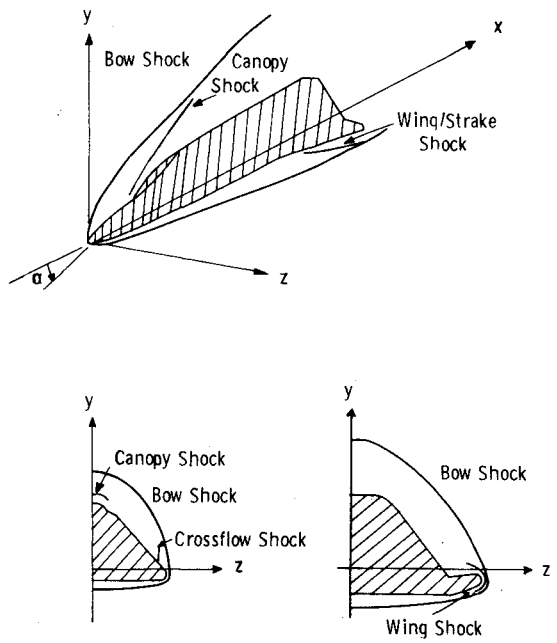

Fig. 1 Complex flowfield over lifting re-entry vehicles.

calculations. This interaction procedure becomes inaccurate for re-entry flowfields, where the viscous effects are not limited to a thin boundary layer, but are important throughout the entire flowfield. Hence, attention has been focused on using a single set of equations valid throughout the flowfield and a parabolic approximation in the streamwise direction such that efficient marching-type techniques could be used.

One such approach was developed by Lubard and Helliwell.[1] The viscous streamwise derivatives were neglected in the Navier-Stokes equations, making them parabolic in the streamwise direction, and the resulting equations are known as parabolized Navier-Stokes (PNS) equations. The PNS equations model most of the features of the re-entry flowfield, except for separated regions in the streamwise direction. These regions occur near the base of the vehicles and are usually small compared to the whole flowfield. The PNS equations have been used by a number of investigators[2-4] to obtain the flowfields over re-entry vehicles of various geometries. The computing times presented in Ref. 2 indicated that solutions required several hours (typically 3-5 hours on an IBM 370/158) and thus too long for design applications.

A second approach—the viscous shock-layer (VSL3D)—was developed by Murray and Lewis[5] for three-dimensional flows. The viscous shock-layer approach was first developed for axisymmetric flows by Davis.[6] The viscous shock-layer equations were also used to obtain a starting solution for the PNS solution.[2] Waskiewicz and Lewis[7] developed a coupling scheme for the continuity and normal momentum equations and obtained significant improvements in the solution of axisymmetric viscous shock-layer flows over spheres. For the first time, Murray and Lewis[5] extended the fully viscous shock-layer equations to three-dimensional flows. The viscous shock-layer equations are derived from Navier-Stokes equations and are parabolic in both streamwise and crossflow directions. Since the crossflow momentum equation is parabolic, the crossflow separated regions on the leeside cannot be treated. Several investigations[8-11] have shown that the three-dimensional viscous shock-layer code (VSL3D) could obtain the solutions in reasonable computing times (typically one hour on an IBM 370/158) and could be used for the design of re-entry vehicles.

Murray and Lewis[8] applied the viscous shock-layer equations to a large number of test cases and validated the method. The body considered was a blunted cone and comparisons with available experimental data were made. In most of these test cases, especially at low Reynolds numbers and moderate angles of attack, the crossflow separated region was small and did not affect the predicted aerodynamic coefficients and heat transfer. However, at high Reynolds number, the crossflow-separated region was large and was cited to be the source of disagreement between the VSL3D predictions and experimental data for the aerodynamic coefficients.

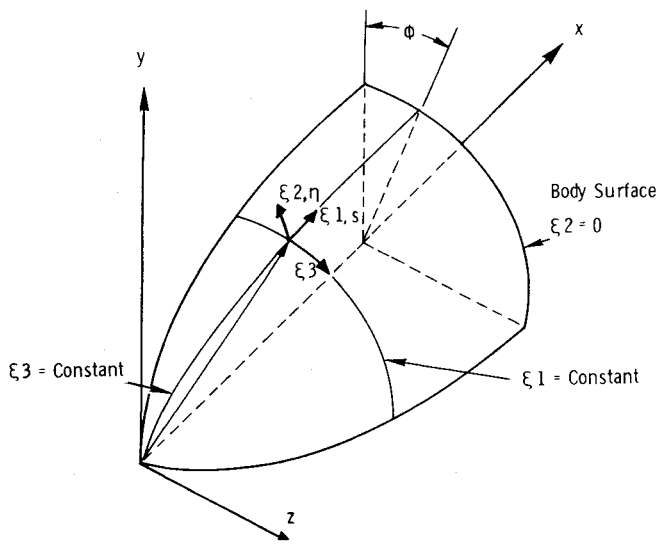

Fig. 2 Coordinate system.

Lifting re-entry vehicles usually have noncircular cross sections including a short wing/strake. A sketch of a typical lifting re-entry vehicle is shown in Fig. 1. The crossflow-separated region on these vehicles will form a major part of the total flowfield and cannot be ignored. The purpose of the research reported here is to include the crossflow-separated region and obtain complete flowfield solutions in reasonable computing times. The viscous shock-layer analysis is used on the windward side up to the crossflow separation point, and flowfield data just prior to the separation point are saved. These data are used to start the PNS solution and compute the crossflow-separated region, thus obtaining the complete flowfield solution. This new method will be referred to as VSLPNS. Helliwell[12] has developed an algorithm known as the Pseudo Elimination Method (PEM) and has demonstrated it on model second-order nonlinear partial-differential equations in two independent variables. It was shown that the Pseudo Elimination Method is faster than the Gauss-Seidel Method (GSM) used for the solution of PNS equations by Lubard and Helliwell.[1] The PEM has been developed for three-dimensional PNS equations and applied to blunt cones at large angles of attack to accelerate the PNS solutions.

The VSLPNS method has been applied to the solution of the complete flowfield over a blunted cone at two flow conditions. The prediction of aerodynamic coefficients for one case is compared with available experimental data. The VSLPNS predictions are also compared with complete PNS and inviscid solutions. The computing times for VSLPNS, VSL3D, and PNS solutions are presented.

Analysis

Coordinate System

The definition of a computational grid is one of the most crucial steps in the building of a numerical technique. The computations are simplified if a body-normal coordinate system is used instead of the usual Cartesian x,y,z or cylindrical x,r,ϕ coordinate system. A body-normal curvilinear coordinate system $\xi 1$, $\xi 2$, $\xi 3$ is shown in Fig. 2. One coor-

dinate, $\xi 3$, is obtained from the intersection of the body's surface with a plane, which makes an angle with the x-y plane. The second coordinate $\xi 1$ is obtained from the condition of orthogonality on the body surface, which then forms the $\xi 1$-$\xi 3$ plane. The third coordinate, $\xi 2$, is the normal to the body surface.

The body shape usually is described in a Cartesian or cylindrical coordinate system. The forces and moments on the body also are expressed in the Cartesian coordinate system. This requires the flowfield, which is computed in the body-normal coordinate system, to be related to the Cartesian/cylindrical coordinate system. The coordinate relations and the metric coefficients $h1$, $h2$, $h3$ are presented in Ref. 13.

General body shapes could be considered with the help of the metrics, since the governing equations have been derived in a general orthogonal curvilinear coordinate system. At present the axisymmetric shock-layer equations are solved to start the solution over a spherical nose. More general nose shapes could be treated by solving the three-dimensional stagnation-point equations.

Governing Equations

Viscous Shock-Layer Equations

The steady laminar viscous shock-layer equations are derived from the steady laminar Navier-Stokes equations in conservation form and in an orthogonal curvilinear coordinate system. These equations are first nondimensionalized by variables which are $\mathcal{O}(1)$ in the flowfield. The normal velocity v and the normal coordinate $\xi 2$ are assumed to be of order ϵ (see Nomenclature). Then terms of second order in ϵ are retained in the $\xi 1$ and $\xi 3$ momentum and energy equations. The conservation equations are then normalized by the local shock values of the flow variables, except for the normal velocity v and the crossflow velocity w, to aid in the solution procedure. The resulting equations are parabolic in the $\xi 1$ and $\xi 3$ directions. Only terms of first order in ϵ are retained in the normal momentum equation. The second-order terms if retained make the normal momentum equation elliptic and difficult to solve. The viscous shock-layer equations are a single set of equations, parabolic in both streamwise and crossflow directions, and valid throughout the flowfield from the body's surface to the bow shock. The parabolic nature does not allow treatment of separated regions in either streamwise or crossflow directions. The complete set of viscous shock-layer equations can be found in Ref. 8.

Parabolized Navier-Stokes Equations

The parabolized Navier-Stokes equations are derived from laminar steady Navier-Stokes equations by assuming the viscous streamwise derivatives small compared to the viscous normal and circumferential derivatives. The resulting equations are parabolic in the streamwise direction and elliptic in the crossflow direction. In addition to the usual boundary-layer order of magnitude of terms, $d\phi$ is assumed to be $\mathcal{O}(\epsilon)$ to include crossflow separation and reverse flow on the leeside and the normal velocity v is taken as $\mathcal{O}(1)$. The flow variables are nondimensionalized bs their freestream values. The normal coordinate is normalized by the shock-layer thickness to facilitate the computation of the shock location. The complete set of parabolized Navier-Stokes equations can be found in Ref. 1.

Boundary Conditions

The re-entry flowfields at high altitudes include low Reynolds number flows where low-density effects such as slip and temperature jump are important. In addition, ablation of body material due to severe aerodynamic heating introduces large mass transfer affecting the flowfield. The shock boundary conditions obtained by classical Rankine-Hugonoit equations have to be modified to account for slip. The shock conditions, which are written in a shock-normal coordinate system, were rotated into the body-normal coordinate system to relate to the flowfield.

The boundary conditions on $\xi 3$ are those of symmetry at $\xi 3 = 0$ and π, which imply that the first derivative of the flow variables u, v, p, h, and β with respect to $\xi 3$ is zero. Also, w and its second derivative with respect to $\xi 3$ are zero. All these boundary conditions were incorporated in the viscous shock-layer procedure[8]; however, the slip conditions at the wall and shock boundaries are not included in the parabolized Navier-Stokes equations.

Solution Procedure

The flowfield between the body and bow shock is divided into a grid of points which are intersections of the coordinate directions s,n,ϕ. The partial derivatives in the governing equations are represented by their finite differences. The details of the solution procedure can be found in Ref. 8 for viscous shock-layer equations and in Ref. 1 for parabolized Navier-Stokes (PNS) equations. The Gauss-Seidel Method[14] (GSM) used to solve PNS equations[1] has been found to have an upperbound on the marching stepsize. An alternate method, known as the Pseudo Elimination Method (PEM), suggested by Helliwell,[12] has been developed for the three-dimensional PNS equations. PEM is a strongly implicit method, hence, the upperbound on the marching stepsize will be larger than that on GSM. The details of the iterative algorithm can be found in Ref. 13. The results of this solver (PEM), when applied to the three-dimensional flow over blunt cones, are presented in later sections.

The VSLPNS method used the viscous shock-layer approach (VSL3D) to obtain the solution on the windward side up to the crossflow separation point. When computing the solution at a ϕ-plane where crossflow separation is imminent, VSL3D fails to obtain a converged solution. No further computations are done toward the leeside at this s station, and the solution is marched down to the next s station. At this new s station, the solution is computed up to the plane at which a successful solution was obtained at the previous s station. When the solution starts dropping planes, it indicates the onset or the s station of the crossflow separation. At this station, the data at the previous two s stations are saved (unit 1) to be used later to start the PNS solution. Later, as the VSL3D solution marches downstream, the flowfield data at

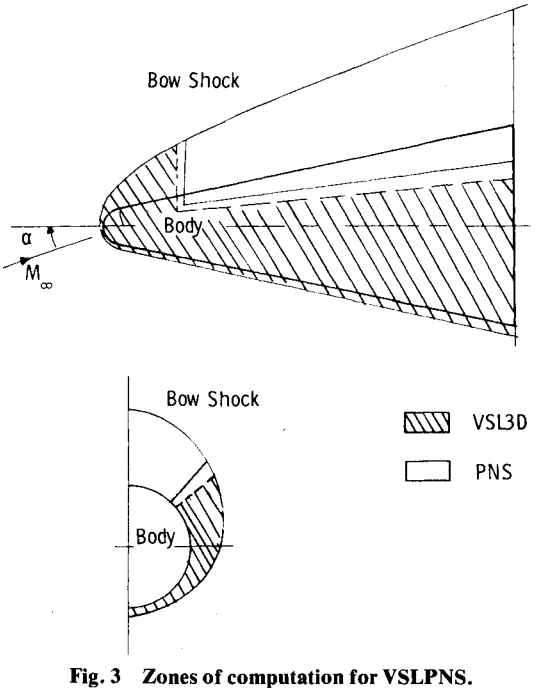

Fig. 3 Zones of computation for VSLPNS.

Table 1 Flow conditions considered

Case	Altitude, ft (m)	Velocity, ft/s (m/s)	Pressure, lb/ft^2 (N/m^2)	Density, slugs/ft^3 (kg/m^3)	Temp., °R (K)	Mach no.	Reynolds no. per ft(m)	Angle of attack, deg	ϵ	T_w/T_0
1	Wind tunnel	4535 (1382)	3.6282 (173.719)	0.261×10^{-4} (0.134×10^{-1})	81 (45)	10	2.0×10^{6} (6.56×10^{6})	10	0.019	0.430
2	245,000 (74,676)	23,297 (7101)	0.0538 (2.5766)	0.867×10^{-7} (0.447×10^{-4})	361.5 (200.8)	25	7.26×10^{3} (2.38×10^{4})	35	0.149	0.018
3	180,000 (54,864)	24,414 (7442)	0.9084 (43.492)	0.111×10^{-5} (0.570×10^{-3})	478.5 (265.9)	23	7.59×10^{4} (2.49×10^{5})	23	0.042	0.012

Table 2 Aerodynamic coefficients for case 1

Coefficient	Experiment	VSLPNS	PNS	VSL3D	Inviscid
C_a	0.1360	0.1314	0.1319	0.1315	0.0965
C_n	0.3050	0.3035	0.3088	0.3157	0.3022
C_m	−0.1976	−0.1968	−0.2016	−0.2086	−0.1972
Z_{cp}/L	0.6485	0.6485	0.6529	0.6607	0.6524

Table 3 Computing times[a] for case 1

Solution	Grid size, Number of n points	ϕ planes	Time, min
VSLPNS + PEM	61	19	94
VSLPNS	101	19	111
PNS	101	19	260
VSL3D	101	10	56

[a] PU time on IBM 370/158, H = OPT2.

the last two planes on the leeside are also saved (unit 2) at each station to be used as the boundary conditions for the PNS solution. The zones of computation are shown in Fig. 3.

The PNS solution uses the flowfield data on unit 1 as the initial conditions and marches down to obtain a solution at the next s station. At this station, the flowfield data on unit 2 for the last two leeside planes are read. It must be noted that the marching stepsize used by VSL3D and PNS differ, requiring interpolation in the streamwise direction. The data read from unit 2 are used to evaluate all of the necessary derivatives at the last plane computed by VSL3D and used as the boundary conditions for the PNS solution. The PNS method then proceeds to obtain the solution from and including this last plane to the leeside plane of symmetry. After obtaining a converged solution, the PNS method marches down to the next s station and the solution procedure is repeated.

The flow variables computed by VSL3D are transformed to correspond to those of PNS before they are written on the units. The integrated aerodynamics coefficients are properly transferred from VSL3D to be continued by PNS.

The surface quantities of engineering interest are the pressure, streamwise and crossflow skin-friction coefficients, and the heat-transfer rate. When slip and mass transfer are included, special relations are used to obtain the surface quantities as given in Ref. 8. The aerodynamic coefficients are obtained by integrating the surface quantities as done by Gogineni and Lewis.[15]

Results and Discussion

The VSLPNS method has been used to solve the complete viscous hypersonic flow over blunted cones at two different flow conditions presented in Table 1. The body considered was a spherically blunted cone with a cone half-angle of 7 deg and 30 nose radii long. The computations were performed on an IBM 370/158, and all the times presented are CPU times on this machine.

Case 1 considered the same flow conditions as those used by Murray and Lewis,[8] in which crossflow separation was cited to be the cause of disagreement in aerodynamic coefficients between the VSL3D predictions and experimental data. The flow conditions are at low Mach number, high Reynolds number, and moderate angle of attack. The complete flowfield was obtained by a PNS solution for purposes of comparison.

For case 1, the crossflow started separating at $s=7.5$ and progressively increased toward the end of the body. At the end of the body, the crossflow-separated region extended from $\phi=142$-180 deg. The complete PNS solution required 260 min of computing time.

Later, the VSLPNS method was used to obtain the solution for case 1. First, the VSL3D solution was obtained. The necessary inviscid shock shape was obtained from an inviscid solution using the computer code described in Ref. 16. The inviscid shock shape on general body shapes could be obtained[17] using the computer code described in Ref. 18.

The computational grid used in presented in Table 3. The stepsize in the marching direction s is controlled by the solution. However, if the solution permits, the s stepsize is increased to a specified maximum. Also, for sphere-cones, the flow over the cone presents less difficulties; therefore, the s stepsize could be increased. In the present case, the maximum stepsize in s direction was allowed to reach about 1.0 without any difficulty in obtaining the solution. The total number of stations in the s direction for the three-dimensional flow calculation was 70. The axisymmetric solution took 18 steps in the s direction.

The VSL3D solution started to have difficulty in computing the solution on the leeside at $s=6.25$, indicating the approach of crossflow separation. An implicit differencing was used to accurately model the streamwise pressure gradient, which is significant on the nose of the body. The VSL3D solution required 56 min of computing time.

Second, the PNS solution was started to complete the crossflow-separated region. The computational grid used is shown in Table 3. The stepsize in the marching direction was chosen to be the maximum allowed for stability criteria given in Ref. 1. A total number of 53 s stations was computed from $s=6.25$-30. Since the PNS solution was started on the cone where the streamwise pressure gradient was not significant, an explicit differencing was used. The PNS solution completed the crossflow-separated region in 56 min of computer time.

The VSLPNS method obtained the complete flowfield, including the crossflow-separated region in 111 min of computing time.

The results of aerodynamic coefficients and computing times for case 1 are summarized in Tables 2 and 3. The results for the axial force C_a, normal force C_n, and pitching moment C_m coefficients and the location of center of pressure Z_{cp}/L are presented for inviscid, VSL3D, PNS, and VSLPNS solutions and experiment. Comparison of inviscid and experimental data indicates a definite presence of strong viscous effects. The agreement between VSL3D and experimental results is better for C_a, C_n than for C_m, Z_{cp}/L. However, the PNS prediction of C_m and Z_{cp}/L shows better agreement with experimental data than the VSL3D prediction, indicating the effect of the crossflow-separated region. The predictions of C_m and Z_{cp}/L by VSLPNS are in much closer agreement with experimental data than VSL3D, confirming that the crossflow-separated region indeed was the cause of the disagreement. It can be observed that the predictions of VSLPNS are in better agreement with experimental data than even the PNS. The reasons for this are that, in the VSLPNS method, the majority of the flowfield was obtained by VSL3D using an accurate implicit formulation of the streamwise pressure gradient, whereas the PNS solution used an explicit formulation.

The computing times indicate that VSLPNS obtained a complete flowfield solution in 111 min, compared to 260 min required for PNS solution—a reduction of 57% in the computing time required.

The shock-layer thickness n_{sh} computed by VSLPNS, VSL3D, and PNS solutions is presented in Fig. 4 which shows the circumferential distribution of n_{sh} at $s=30$. VSL3D obtained the solution up to $\phi=140$ deg, and VSLPNS obtained the solution from $\phi=130$-180 deg. The shock shapes are in good agreement with those of PNS.

The circumferential distribution of the wall pressure at $s=30$ is shown in Fig. 5. The results of VSL3D and PNS agree well on the windward side but not on the leeside at $\phi=140$ deg because of the backward differencing used to evaluate the ϕ derivatives in the VSL3D method. The results of VSLPNS are in close agreement with the PNS predictions on the leeside

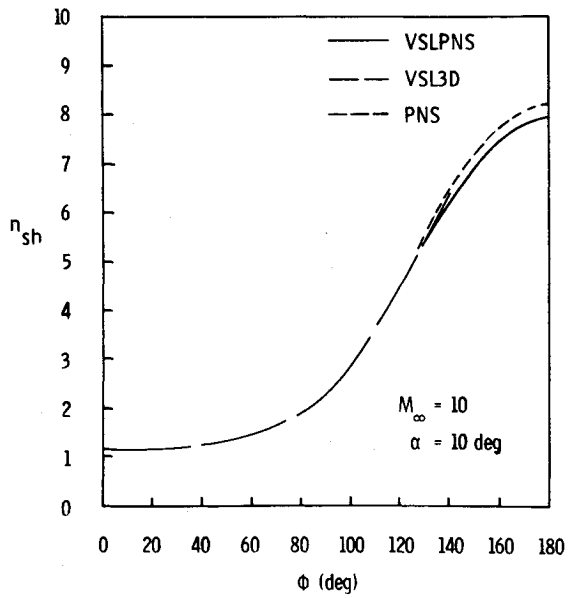

Fig. 4 Circumferential distribution of n_{sh} at $s=30$ for case 1.

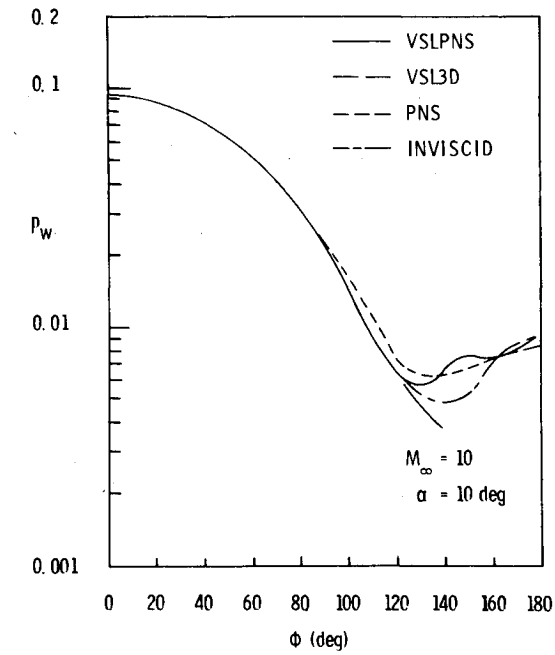

Fig. 5 Circumferential distribution of p_w at $s=30$ for case 1.

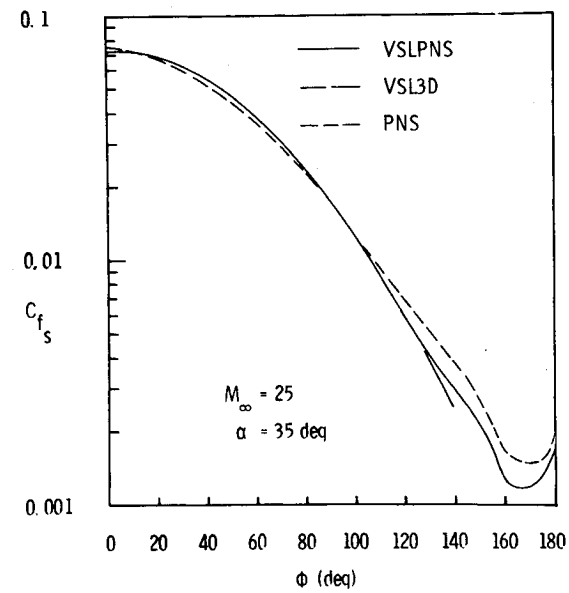

Fig. 6 Circumferential distribution of C_{f_s} at $s=30$ for case 1.

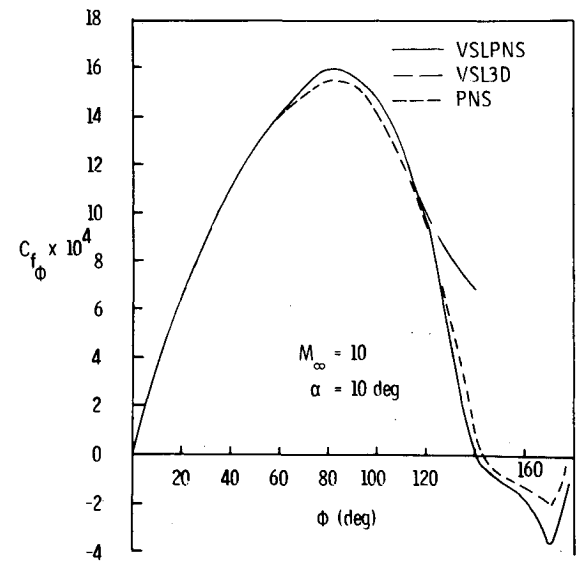

Fig. 7 Circumferential distribution of C_{f_ϕ} at $s=30$ for case 1.

planes $\phi = 140$-180 deg. The VSL3D prediction at $\phi = 140$ deg is significantly lower than the PNS predictions. The VSLPNS prediction shows an oscillatory convergence to the PNS prediction. This result is the effect of not computing the crossflow-separated region, since in that region the wall pressure increases again, as shown by the VSLPNS and PNS prediction. This behavior is typical of the implicit iterative solution of the governing equations with different approximations in conversative form. The boundary data from VSL3D solution will not satisfy the PNS equations, and the iterative solution produced an oscillation.

The circumferential distribution of C_{f_s} at $s = 30$ is shown in Fig. 6. The VSLPNS predictions on the leeside are in close agreement with those of PNS.

The circumferential distribution of crossflow skin-friction coefficient C_{f_ϕ} is shown in Fig. 7. There is considerable difference in the predictions of VSL3D and PNS at $\phi = 140$ deg. In the crossflow-separated region, C_{f_ϕ} changes sign. This region is small and does not affect the axial and normal force coefficients. However, when moments are considered about the nose, it affects the pitching moment coefficient and the center-of-pressure location. The VSLPNS predictions are in close agreement with those of PNS.

The crossflow velocity profiles across the shock layer are shown in Fig. 8 for the leeside planes $\phi = 130$-180 deg. The crossflow velocity is positive in the counterclockwise direction, as indicated by the arrow on the body surface. The slope of the velocity profile at the wall is positive at $\phi = 130$ deg, zero at $\phi = 140$ deg, and negative from $\phi = 150$-170 deg, indicating the onset of crossflow separation at $\phi = 140$ deg. From $\phi = 150$-170 deg, there is reverse flow near the wall showing the presence of the separation bubble. The separation bubble is also shown in Fig. 8.

Case 2 considered high Mach number, low Reynolds number flow at large angle of attack. The crossflow-separated region is smaller than that for case 1 because of the lower Reynolds number. This case has been considered to validate VSLPNS under an entirely different set of flow conditions at the highest angle of attack. The results for aerodynamic coefficients and computing times from VSLPNS, VSL3D, and PNS solutions are presented in Tables 4 and 5. The differences between the predictions of VSL3D, VSLPNS, and PNS are small since the crossflow-separated region is small. The VSLPNS predictions indicate improved agreement with PNS predictions for the center-of-pressure location. The computing times indicate that VSLPNS obtains the complete flowfield solution in 140 min, compared to 324 min required for PNS solution—a reduction of 57% in the computing time required.

Table 4 Aerodynamic coefficients for case 2

Coefficient	VSLPNS	PNS	VSL3D
C_a	0.5582	0.5635	0.5568
C_n	1.5781	1.5841	1.5863
C_m	−0.9803	−0.9952	−1.0025
Z_{cp}/L	0.6212	0.6282	0.6320

Table 5 Computing times[a] for case 2

Solution	Grid size Number of n points	ϕ planes	Time, min
VSLPNS	101	19	140
PNS	101	19	324
VSL3D	101	10	55

[a] CPU time on IBM 370/158, H = OPTZ.

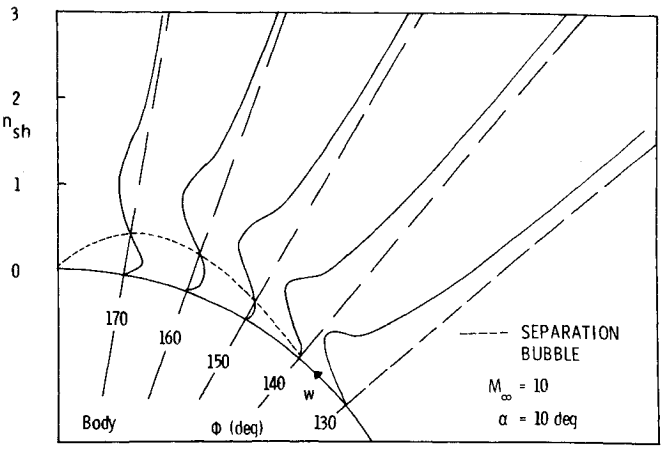

Fig. 8 Crossflow w velocity profiles near the leeside plane of symmetry for case 1.

The PEM solver was first applied to a test case, and studies were made to verify its effectiveness in accelerating the solutions of PNS equations. The flow conditions considered are referred to as case 3 and are given in Table 1. The stepsize studies were limited to the conical portion of the body from $s = 20$-30 to avoid the influence of the blunt nose. The solution obtained by the Gauss-Seidel Method (GSM) of Lubard and Helliwell[1] was used to provide the initial data at $s = 20$ to start the PEM solution. Both implicit and explicit formulations for modeling the streamwise pressure gradient were used. The maximum stepsize (DXMAX) required for stability[1] was used first. Later, the stepsize was increased to twice and thrice DXMAX. The computing times for these stepsize studies are presented in Table 6. The GSM failed to obtain a solution at $2 \times$DXMAX. The PEM obtained solutions at $2 \times$DXMAX faster than GSM at DXMAX. Both PEM and GSM failed to obtain a solution at $3 \times$DXMAX. Explicit or implicit formulation of streamwise pressure gradient did not affect the flow variables, since on this part of the body the streamwise pressure gradient was almost zero.

The solutions over the full length of the body were obtained using both PEM and GSM. The computing times along with the grid size used are shown in Table 7. PEM required 180 min compared to the 260 min required by the GSM, indicating that PEM is faster than GSM in solving the PNS equations by a factor of 1.45. However, the storage requirements for PEM were greater than GSM. This need for increased storage has limited the grid size in the normal direction.

The PEM has also been used to solve the PNS equations for the flow conditions of case 1. The solution was started at $s = 6.25$ and continued to $s = 30$. A marching stepsize of about $3 \times$DXMAX was used. The computing times are shown in Table 7. The PEM required 90 min compared to 140 min required for GSM, indicating that PEM is faster than GSM by a factor of about 1.55. This method was used in VSLPNS, which then obtained the complete solution in 94 min with no plottable difference in the flow variables. Explicit for-

Table 6 Stepsize studies for the Pseudo Elimination Method (PEM)

Stepsize[a]	Time,[b] min PEM Explicit	PEM Implicit	GSM Explicit	GSM Implicit
DXMAX	46	60	39.5	40
$2 \times$DXMAX	26.5	34.5	...	...
$3 \times$DXMAX	...	...	...	...

[a] Grid size: 61 n points, 19 ϕ planes.

[b] CPU time on IBM 370/158, H = OPT2.

Table 7 Computing times[a] for cases 1 and 3 using GSM and PEM[b]

Flow conditions	GSM	PEM	Speed factor
Case 3	260	180	1.45
Case 1	140	90	1.55

[a] CPU time in minutes on IBM 370/158, H = OPT2.
[b] Grid size: case 3 used 61 n points, 19 ϕ planes for GSM and PEM; case 1 used 101 n points, 19 ϕ planes for GSM and 61 n points, 19 ϕ planes for PEM.

mulation of the streamwise pressure gradient was used to facilitate comparisons with the previous PNS solutions.

The convergence criteria (10^{-10}) for the iterative algorithm was the same for both GSM and PEM. However, the grid size used in the normal direction was different, since experience has shown that GSM required a larger number of grid points (101 points) for reliable solutions. The present comparisons are limited, but the conclusions are of practical importance. Further evaluation is necessary to better establish the exact speed ratio between PEM and GSM when applied to bodies with noncircular cross sections.

Conclusions and Recommendations

A procedure (VSLPNS) has been developed to compute for the first time the three-dimensional laminar viscous hypersonic flowfields using the shock-layer approach including the crossflow-separated region.

Comparisons with experimental data indicate that the VSLPNS predictions of aerodynamic coefficients are accurate, and the crossflow-separated region has a significant effect on the coefficients. This result supports the view that the crossflow-separated region will be very important for flows over lifting re-entry vehicles having triangular cross sections or high Reynolds number flows at moderate angles of attack.

A new solver, called the Pseudo Elimination Method, has been developed for solving the three-dimensional parabolized Navier-Stokes equations. This solver accelerated the solution by a factor of 1.55 in one case, compared to a previous solution using the Gauss-Seidel method of Lubard and Helliwell.[1]

Comparisons with the parabolized Navier-Stokes solution indicate that VSLPNS predicts the flowfield data accurately in much less time. This computing advantage makes VSLPNS attractive for design applications of lifting re-entry vehicles where large crossflow-separated regions exist. A procedure has been indicated to apply the VSLPNS method for general body shapes.

Further work is required to include slip boundary conditions in the parabolized Navier-Stokes equations so that VSLPNS could be applied to flow conditions where slip effects are significant. The three-dimensional stagnation point viscous shock-layer equations must be solved to include more general nose shapes.

References

[1] Lubard, S.C. and Helliwell, W.S., "Calculation of the Flow on a Cone at High Angle of Attack," *AIAA Journal*, Vol. 12, July 1974, pp. 965-974.

[2] Waskiewicz, J.D. and Lewis, C.H., "Hypersonic Viscous Flows over Sphere-Cones at High Angles of Attack," AIAA Paper 78-64, Jan. 1978.

[3] Agopian, K., Collins, J., Helliwell, W., Lubard, S.C., and Swan, J., "NASA Viscous 3-D Flowfield Calculations," R&D Associates, RDA-TR-6100-007, Oct. 1975.

[4] Mayne, A.W., Jr., "Calculation of the Laminar Viscous Shock Layer on a Blunt Biconic Body at Incidence to Supersonic and Hypersonic Flow," AIAA Paper 77-88, Jan. 1977.

[5] Murray, A.L. and Lewis, C.H., "Viscous Shock-Layer Flows over Bodies during Reentry," AIAA Paper 78-259, Jan. 1978.

[6] Davis, R.T., "Numerical Solution of the Hypersonic Viscous Shock Layer Equations," *AIAA Journal*, Vol. 8, May 1970, pp. 843-851.

[7] Waskiewicz, J.D., Murray, A.L., and Lewis, C.H., "Hypersonic Shock-Layer Flow over a Highly Cooled Sphere," *AIAA Journal*, Vol. 16, Feb. 1978, pp. 189-192.

[8] Murray, A.L. and Lewis, C.H., "Three-Dimensional Fully Viscous Shock-Layer Flows over Sphere Cones at High Altitudes and High Angles of Attack," Aerospace and Ocean Engineering Dept., Virginia Polytechnic Institute and State University, Blacksburg, Va. VPI&SU AERO-78, Jan. 1978.

[9] Gogineni, P.R., Murray, A.L., and Lewis, C.H., "Viscous Flows over Spherically Blunted Cones at Large Angle of Attack Including Mass-Transfer and Low Reynolds Number Effects," AIAA Paper 78-1188, July 1978.

[10] Murray, A.L. and Lewis, C.H., "Heat- and Mass-Transfer Effects on Three-Dimensional Hypersonic Viscous Shock-Layer Flows," AIAA Paper 78-844, May 1978.

[11] Lewis, C.H., Gogineni, P.R., and Murray, A.L., "Comparison of Viscous Shock-Layer Predictions with Experiment for Blunted Cones in Rarefied Transition Regime," Paper 157, 11th International Symposium on Rarefied Gasdynamics, Cannes, France, July 1978.

[12] Helliwell, W.S., "Fast Implicit Iterative Numerical Method for Solving Multidimensional Partial Differential Equations," *AIAA Journal*, Vol. 16, July 1978, pp. 663-666.

[13] Gogineni, P.R. and Lewis, C.H., "VSLPNS: Three-Dimensional Viscous Hypersonic Flow Predictions Using Combined Shock-Layer and Parabolized Navier-Stokes Equations," Aerospace and Ocean Engineering Dept., Virginia Polytechnic Institute and State University, Blacksburg, Va., VPI-AERO-094, April 1979.

[14] Isaacson, E. and Keller, H.B., *Analysis of Numerical Methods*, John Wiley and Sons, Inc., New York, 1966, pp. 58-60.

[15] Gogineni, P.R. and Lewis, C.H., "A Computer Program to Calculate Aerodynamic Coefficients of Spherically Blunted Cones at Angle of Attack with Asymmetric Mass Transfer," Aerospace and Ocean Engineering Dept., Virginia Polytechnic Institute and State University, Blacksburg, Va., VPI-AERO-086, Feb. 1978.

[16] Solomon, J.M., Ciment, M., Ferguson, R.E., Bell, J.B., and Wardlaw, A.B., Jr., "A Program for Computing Steady Inviscid Three-Dimensional Supersonic Flow on Reentry Vehicles, Vol. 1, Analysis and Programming," Naval Surface Weapons Center, White Oak, Silver Spring, Md., NSWC/WOL/TR 7728, Feb. 1977.

[17] Hamilton, H.H., private communications, NASA Langley Research Center, Hampton, Va., Dec. 1978.

[18] Marconi, F., Salas, M., and Yaeger, L., "Development of a Computer Code for Calculating the Steady Super/Hypersonic Inviscid Flow Around Real Configurations, Vol. I, Computational Technique," NASA CR-2675, April 1976.